Li, Yun; Yang, Shenghai; Taskinen, Pekka; He, Jing; Liao, Fangwen; Zhu, Rongbo; Chen, Yongming; Tang, Chaobo; Wang, Yuejun; Jokilaakso, Ari

Novel recycling process for lead-acid battery paste without SO_2 generation - Reaction mechanism and industrial pilot campaign

Published in:
Journal of Cleaner Production

DOI:
10.1016/j.jclepro.2019.01.197

Published: 20/04/2019

Document Version
Peer-reviewed accepted author manuscript, also known as Final accepted manuscript or Post-print

Number of words 6527

Novel recycling process for lead-acid battery paste without SO_2 generation - Reaction mechanism and industrial pilot campaign

Yun Li [a,b], Shenghai Yang [a], Pekka Taskinen [b], Jing He [a], Fangwen Liao [a], Rongbo Zhu [a], Yongming Chen [a,*], Chaobo Tang [a,*], Yuejun Wang [c,*], Ari Jokilaakso [a,b,*]

[a] *School of Metallurgy and Environment, Central South University, Changsha, Hunan, 410083, China,*

[b] *Aalto University, School of Chemical Engineering, Department of Chemical and Metallurgical Engineering, Espoo, 02150, Finland,*

[c] *Hetao College, Department of Ecology and Resources Engineering, Bayannur, China*

ABSTRACT

This study proposes an innovative and environment-friendly method for recycling spent lead-acid batteries without SO_2 generation. Iron-containing waste was employed as a sulfur-fixing agent to retain sulfur as ferrous matte, which eliminated the generation and emissions of gaseous SO_2. This work investigated the thermodynamic and experimental feasibility and conversion mechanism of the method, and evaluated its industrial applicability. A bench-scale test showed direct recoveries of 93.5 % and 97.7% in crude lead and ferrous matte for lead and sulfur, respectively. The phase transformation mechanism study indicated that metallic lead from the lead paste was extracted mainly through the sequence of $PbSO_4 \xrightarrow{C/CO} PbS \xrightarrow{Fe_3O_4} PbO \xrightarrow{C/CO} Pb$. Sulfur in $PbSO_4$ was thus first transferred to PbS and finally fixed as FeS. An industrial-scale pilot campaign was also conducted to confirm the feasibility and reliability of the new process.

Keywords: reductive sulfur-fixing smelting; efficient lead extraction; reaction mechanism; SO_2 emission; industrial application evaluation.

List of abbreviations

LAB --- lead-acid battery;
ICP-AES --- Inductively Coupled Plasma-Atomic Emission Spectrometry;
XRD --- X-ray diffraction;
FC_d --- fixed carbon;
Vd --- dry basis volatiles;
A_d --- dry basis ash;
TG-DTA --- Thermogravimetric Analysis- Differential Thermal Analysis;
SEM-EDS --- Scanning Electron Microscope and Energy Diffraction Spectrum.

* Corresponding author. School of Metallurgy and Environment, Central South University, Changsha, Hunan, 410083, China.
E-mail addresses: csuchenyongming@163.com (Y.M. Chen); chaobotang@163.com (C.B. Tang); thirtythree61@aliyun.com (Y.J. Wang); ari.jokilaakso@aalto.fi (Ari Jokilaakso).

1. Introduction

Lead is used in lead-acid batteries (LABs) (Dahodwalla and Herat, 2000), in building and military applications, and in various alloys. Advances in the automobile, chemical, energy, transportation, and telecommunication industries are increasingly expanding both the demand for lead and also its scrap volume growth worldwide (Tian et al., 2015). The annual amount of LAB scrap in China is more than 2.6 Mt, around 1.79 Mt in the Americas, and approximately 1.5 Mt in Europe (Tian et al., 2015; Zhang, 2013). In addition, considering the shortage of primary lead ores, increasing interest is being shown in recycling lead from secondary resources, including LABs, lead-bearing sludges, glass, and the dusts and slags produced in various metallurgical processes.

LAB scrap is a significant secondary lead source worldwide (Zhang, 2013). Lead produced in recycling now dominates the world's lead market (Ellis and Mirza, 2010). More than 95% of the LABs used in the US and Europe are recycled (Higgins, 2007; Kreusch et al., 2007). In China, the recycling degree of lead-bearing secondary materials is alarmingly low: the production of secondary lead in 2015 was approximately 1.85 Mt, accounting for only 40% of lead production (Tian et al., 2015). More effort is needed to develop economic and environment-friendly recycling technologies for lead secondaries.

An end-of-life LAB consists of four main components: waste electrolyte (11-30%), polymeric materials (22-30%), lead alloy grids (24-30%), and lead paste (30-40%). Of these, lead paste is the most difficult to recycle. It is a mixture of 50-60% $PbSO_4$, 15-35% PbO_2, 5-10% $PbO/Pb(OH)_2$, 2-5% metallic Pb, and a small amount of impurities, such as iron, antimony, tin, and barium (Lin and Qiu, 2011). However, it is a high-quality lead-bearing material.

LAB recycling technology can be divided into the traditional routes of pyrometallurgy and hydrometallurgy, and advanced approaches including electrowinning (Andrews et al., 2000), biological techniques (Schröder-Wolthoorn et al., 2008), and vacuum methods (Lin and Qiu, 2011). In hydrometallurgy (Pan et al., 2016; Singh, 2015), Na_2CO_3, NaOH, and K_2CO_3 solutions or citric acid and citrate are employed as desulfurizing reagents. Hydrometallurgical desulfurization (Karandikar, 2015) has been widely adopted for battery recycling in western countries thanks to its environmental advantages (Hotea, 2013).

In spite of increasing attention on hydrometallurgical recycling (Ma et al., 2016), pyrometallurgy is still the predominant methodology worldwide (Kreusch et al., 2007). It seems to be more appropriate for the Chinese lead industry (Tian et al., 2014; Zhang, 2013), because it is proven, simple, and economical. In addition, considering the shortage and high price of electricity in China, the operational cost of the hydrometallurgical methods is high (Zhang, 2013). In the secondary lead industry, a blast furnace, electric furnace, reverberatory furnace, converter furnace, or short rotary furnace is employed to smelt lead paste to produce antimony-bearing lead bullion and soda slag or matte (Kreusch et al., 2007; Queneau et al., 2015). Some smelters also feed small amounts of lead paste (generally less than 20%) together with galena concentrate in primary smelting (Zhang, 2013). The pyrometallurgical recycling of LABs includes smelting after pre-desulfurization (Gong et al., 2015) at low temperatures or direct smelting of lead paste without desulfurization at temperatures above 1000°C (Jeong and Kim, 2017). However, these technologies do not focus on the recovery of sulfur; sulfur dissolves into the crude metal during the desulfurization process and reacts to form gaseous SO_2 during smelting.

Pyrometallurgical treatment of spent LABs always involves a potential health and environmental risk (Tian et al., 2017; Van der Kuijp et al., 2013). Therefore, the lead recycling industry is keen to seek novel technologies to treat secondary materials economically, reduce energy usage and production cost, and minimize environmental pollution (Jaeck, 2013; Wei et al., 2014). This includes the storage of lead residues, and emissions of lead-containing particle dusts and SO_2 gas (Kreusch et al., 2007; Sonmez and Kumar, 2009).

For the above reasons, an innovative and cleaner pyrometallurgical process was proposed to promote lead extraction from secondary materials through reductive smelting (Li et al., 2017; Ye et al., 2015). The novelties of this process were sulfur fixation and recycling, co-treatment of iron-containing solid wastes, a shorter flowsheet, and wide adaptability for secondary materials. After several years of laboratory studies (Huang et al., 2012; Tang et al., 2004), this process is in use in a number of recycling plants in China (Guoda Nonferrous Metals Smelting Co., 2009); (Guangdong Xinsheng Environmental Science & Technology Co., 2014).

In this study, the fundamental conversion mechanisms and reaction paths of reductive smelting were further examined. In addition, a lab-scale process

optimization and an industrial application trial campaign were completed and evaluated.

2. Materials and methods

2.1 Materials

Spent lead paste was obtained from Yuguang Gold & Lead Co., Henan, China. Iron-oxide-rich hematite and coke were supplied by Xiangtan Iron & Steel Co., Ltd of Hunan Valin, China. The chemical compositions of these materials were analyzed by Inductively Coupled Plasma-Atomic Emission Spectrometry (ICP-AES, Perkin Elmer, Optima 3000; Norwalk, USA). The results are shown in Table 1. The X-ray diffraction (XRD) results of the lead paste and hematite are illustrated in Figure 1. They indicate that the hematite contained 88.0% Fe_2O_3 (total iron 64.8%) and that the main impurity was SiO_2. The lead paste contained 72.9% lead and 4.7% sulfur. The main lead-bearing phases in the lead paste were $PbSO_4$ (54.7%), PbO_2 (22.1%), metallic Pb (8.5%), and PbO (8.5%).

Table 1. Chemical analysis of raw materials /wt.% .

Materials	TPb	S	Fe	Zn	Ca	Sn	Na	Mg	Al	Ba	Sb
Lead paste	72.90	4.69	0.02	0.01	0.16	0.05	0.33	0.05	0.05	0.15	0.07
	$PbSO_4$	PbO	PbO_2	Pb							
	54.68	8.49	22.05	8.53							
Hematite	Fe_2O_3	S	TFe	Zn	CaO	SiO_2	Na	MgO	Al_2O_3		
	87.98	0.025	64.81	0.01	0.28	8.96	0.042	0.78	1.67		
Coke	Industrial analysis/%			Chemical composition of the ash/%							
	FC_d	V_d	A_d	Fe_{total}	SiO_2	CaO	Al_2O_3	MgO			
	81.27	3.30	15.43	25.23	41.23	6.60	25.24	0.53			

FC_d: fixed carbon; Vd: dry basis volatiles; A_d: dry basis ash.

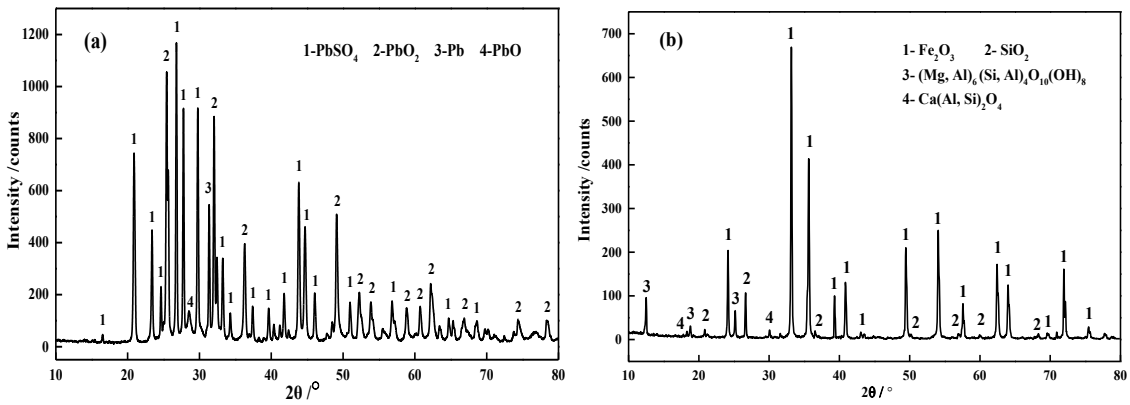

Fig. 1. XRD patterns of (a) lead paste and (b) hematite

Analytical purity materials, including $PbSO_4$ powder, ferric oxide Fe_2O_3, carbon, SiO_2, and CaO, were purchased from Aladdin Industrial Corporation (China). The materials were pre-ground to a particle size passing through a 200-mesh screen (<0.074 mm). The argon gas used for protection during the reaction was more than 99.99 vol% pure.

Figures 2 (a)-(c) show the thermogravimetric analysis (TG-DTA, STA 494 F3; NETZSCH, Germany) curves of the $PbSO_4$ powder, $PbSO_4$-C, and $PbSO_4$-Fe_2O_3-C mixtures. The TG curve of $PbSO_4$ in Figure 2 (a) shows two different zones within the tested temperature range. First, 0.9% of the weight loss appeared at 145°C (418 K) and peaked at 202°C (475 K), generating a small endothermic peak. This weight loss was associated with vaporization of crystalline water. The main weight loss was recorded from 808°C (1081 K) to 1001°C (1274 K), with a total loss of 14.7%. Two pronounced endothermic peaks were observed at 879°C (1152 K) and 971°C (1244 K), associated with the volatilization and decomposition reactions of $PbSO_4$.

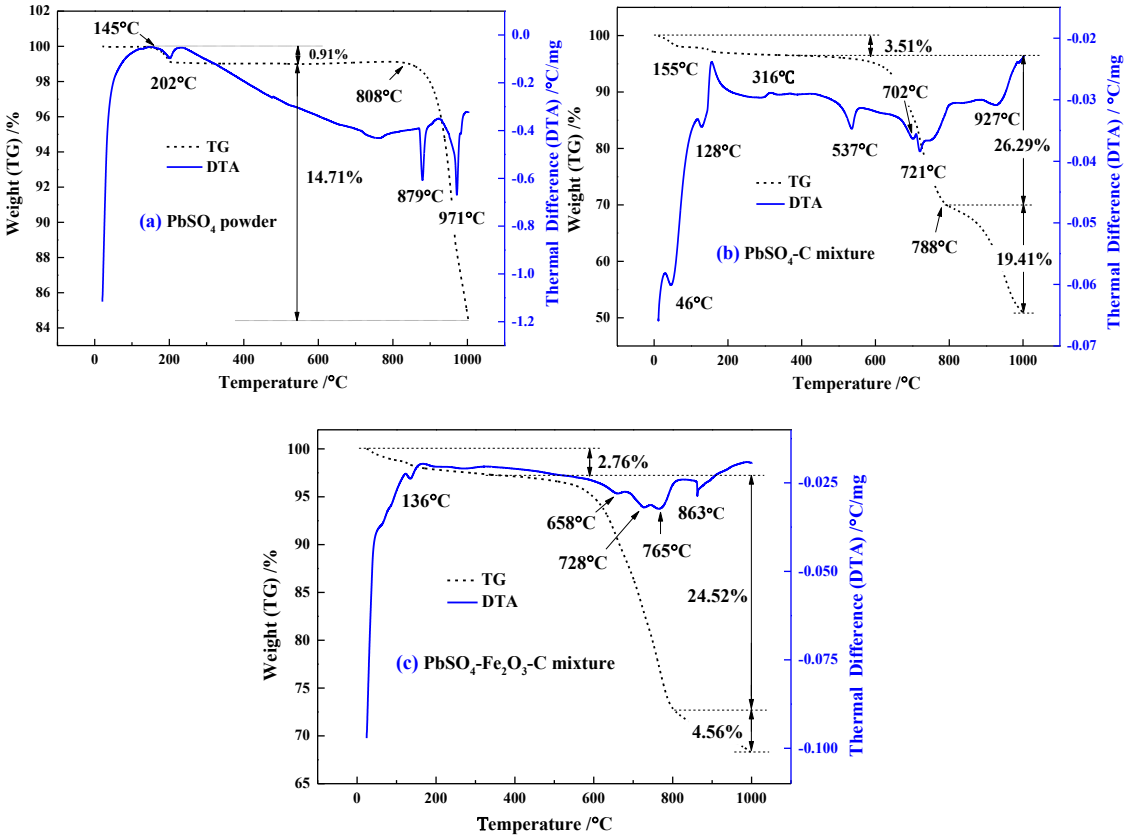

Fig. 2. TG-DTA results of (a) $PbSO_4$ powder, (b) $PbSO_4$-C mixture (molar ratio 1:6), and (c) $PbSO_4$-Fe_2O_3-C mixture (molar ratio 2:1:12) in Ar gas (heating rate 10 °C/min, Ar flow 100 mL/min)

The TG-DTA of the $PbSO_4$-C and $PbSO_4$-Fe_2O_3-C mixtures shown in Figures 2 (b) and (c) illustrate that there were three mass loss processes. The first weight loss of 3.5% in the $PbSO_4$-C mixture and 2.7% in the $PbSO_4$-Fe_2O_3-C mixture were associated with the loss of water. The major weight loss in both systems was recorded in the second step. In the $PbSO_4$-C mixture, a distinct 26% weight loss began at 537°C (810 K) and ended at 788°C (1061 K). This was assumed to be the decomposition of $PbSO_4$ and consumption of carbon. Two weak endothermic peaks were observed at 702°C and 721°C, associated with the reaction of $PbSO_4$. In the $PbSO_4$-Fe_2O_3-C system, 29% of the weight loss was recorded in the second zone. Two weak endothermic and one relatively strong endothermic peaks were detected at 658°C (931 K), 728°C (1001 K), and 765°C (1038 K), respectively. They were related to solid-state reactions in the mixture. A pronounced endothermic peak was recorded at 863°C (1136 K) in connection with the final 4.5% weight loss, which corresponded to reactions occurring in the molten PbO-$PbSO_4$. The third weight loss in the $PbSO_4$-C mixture (19%) was recorded from 788°C (1061 K) to 1000°C (1273 K). An endothermic peak was detected at 927°C (1200 K), assumed to be due to the reduction-decomposition reaction of $PbSO_4$. The total of 49% weight loss in the $PbSO_4$-C mixture was larger than that in the $PbSO_4$ system, even after deducting the loss of additional carbon. This indicates that the presence of reductant promoted $PbSO_4$ decomposition.

2.2 Methods

In the lab-scale batch experiments, 300 g of lead paste was mixed with a given amount of coke, hematite, and other fluxes (SiO_2 and CaO), and the mixture was placed in an alumina crucible. The crucible was pushed into the constant temperature zone of the furnace at the desired temperature. After the required smelting time, the crucible was taken out and quickly quenched in liquid nitrogen and weighed. The crucible was broken to carefully separate and weigh the crude lead, ferrous matte, and slag. The separated layers were then crushed and prepared for ICP-AES analysis. The direct Pb recovery rate (γ) and sulfur-fixing rate (ξ) were calculated based on the following equations:

$$\gamma = \frac{Mass\ of\ Pb\ in\ the\ crude\ lead}{Mass\ of\ Pb\ in\ the\ initial\ feeding\ materials} \times 100\%$$

$$\xi = \frac{Mass\ of\ sulfur\ in\ the\ ferrous\ matte\ and\ slag}{Mass\ of\ sulfur\ in\ the\ inital\ feeding\ materials} \times 100\%$$

In the reaction mechanism experiments, synthetic $PbSO_4$ powder was selected as the raw material, since it is the major as well as the most difficult component to deal with in the spent lead paste. It was mixed with carbon and ferric oxide according to the stoichiometries of their possible reactions. First, a small amount of mixture was analyzed using TG-DTA at a heating rate of 10 °C/min and Ar flow of 100 mL/min from 25°C to 1000°C. The remaining mixtures were pressed uniaxially under 15 MPa pressure into cylindrical samples of 10 mm diameter. The samples were put into a 10 mL alumina crucible and pushed slowly into the constant temperature zone of the furnace (as shown in Figure 3), after flushing away air with Ar, and held there for a preset time. The temperature was measured with a Pt–Rh thermocouple and controlled using a SHIMADEN SR25 Intelligent Temperature Controller (accuracy ± 1°C; Japan). The Ar gas flow was fixed to 1.0 L/min.

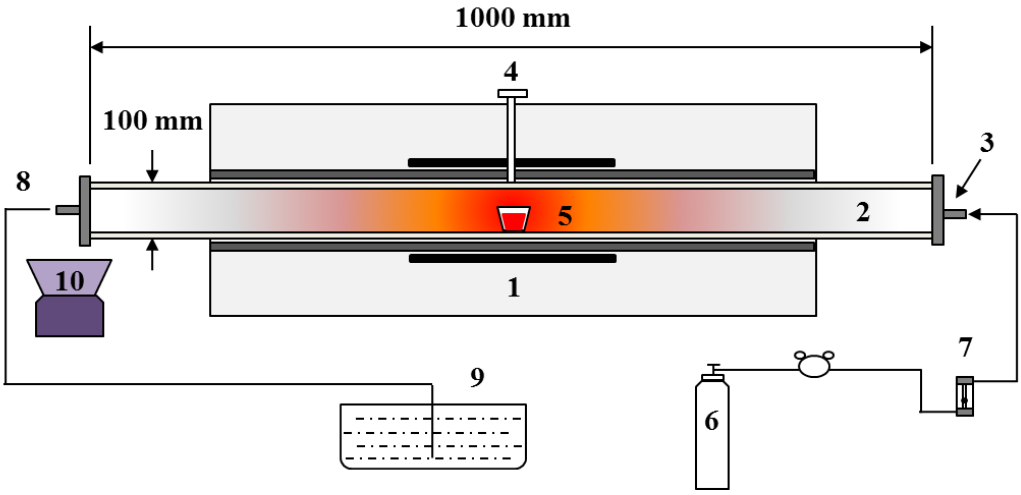

(1) Horizontal tube furnace; (2) Alumina work tube; (3) Sealing flange; (4) Pt-PtRh thermocouple; (5) Alumina crucible; (6) Ar gas cylinder; (7) Flowmeter; (8) Off gas; (9) Alkali liquor vessel; (10) Liquid-nitrogen cooling device.

Fig. 3. Schematic of the experimental apparatus.

After polishing, the samples were carbon coated and analyzed immediately. The phase compositions and microstructures were determined by XRD and Scanning Electron Microscope and Energy Diffraction Spectrum analysis (SEM-EDS, LEO 1450, Carl Zeiss, Germany; EDS, INCA Wave 8570, Oxford Instruments, UK), respectively. The remaining samples were ground to a particle size of less than 0.074 mm for XRD analysis. The XRD profiles of the samples were measured using an X-ray diffractometer (XRD, D/max 2550PC, Rigaku Ltd; Japan) with Cu Ka radiation. The data were collected in the range of 2θ=10–80° with a 2θ step width

of 1°. The recorded patterns were evaluated using the PDF-2 powder diffraction pattern database (Toby, 2005). The determination of different phases in the SEM images was based on EDS analysis results of 10 different points in the same mineral.

3. Thermodynamic calculation

$PbSO_4$ can react in reducing atmospheres with the sulfur-fixing agent hematite (Fe_2O_3) to produce metallic Pb and FeS. The sulfur in $PbSO_4$ will be transferred to FeS and ultimately fixed. As intermediate products, $PbSO_4$ and Fe_2O_3 will be reduced to PbS and Fe_3O_4, respectively. The various reaction paths can be briefly represented with the reactions shown in Table 2.

Table 2. Possible reactions taking place in the reductive sulfur-fixing smelting process of lead paste ($\Delta G_T^\theta/(kJ/mol); T/°C$).

$2PbSO_4 + Fe_2O_3 + 11\ C = 2Pb + 2FeS + 11\ CO_{(g)}$	$\Delta G_T^\theta = -1.958\ T + 669.86$	(1)
$2PbSO_4 + Fe_2O_3 + 11\ CO_{(g)} = 2Pb + 2FeS + 11\ CO_{2(g)}$	$\Delta G_T^\theta = 0.025\ T - 738.06$	(2)
$3PbSO_4 + Fe_3O_4 + 16\ C = 3Pb + 3FeS + 16\ CO_{(g)}$	$\Delta G_T^\theta = -2.808\ T + 964.2$	(3)
$3PbSO_4 + Fe_3O_4 + 16\ CO_{(g)} = 3Pb + 3FeS + 16\ CO_{2(g)}$	$\Delta G_T^\theta = 0.062\ T - 1076.7$	(4)
$PbSO_4 + 4\ C = PbS + 4\ CO_{(g)}$	$\Delta G_T^\theta = -0.681\ T + 166.39$	(5)
$PbSO_4 + 4\ CO_{(g)} = PbS + 4\ CO_{2(g)}$	$\Delta G_T^\theta = 0.025\ T - 331.38$	(6)
$2PbS + Fe_2O_3 + 3C = 2Pb + 2\ FeS + 3\ CO_{(g)}$	$\Delta G_T^\theta = -0.589\ T + 335.2$	(7)
$2PbS + Fe_2O_3 + 3\ CO_{(g)} = 2Pb + 2FeS + 3\ CO_{2(g)}$	$\Delta G_T^\theta = -0.064\ T - 32.355$	(8)
$3PbS + Fe_3O_4 + 4\ C = 3Pb + 3FeS + 4\ CO_{(g)}$	$\Delta G_T^\theta = -0.765\ T + 465.04$	(9)
$3PbS + Fe_3O_4 + 4\ CO_{(g)} = 3Pb + 3FeS + 4\ CO_{2(g)}$	$\Delta G_T^\theta = -0.066\ T - 24.184$	(10)

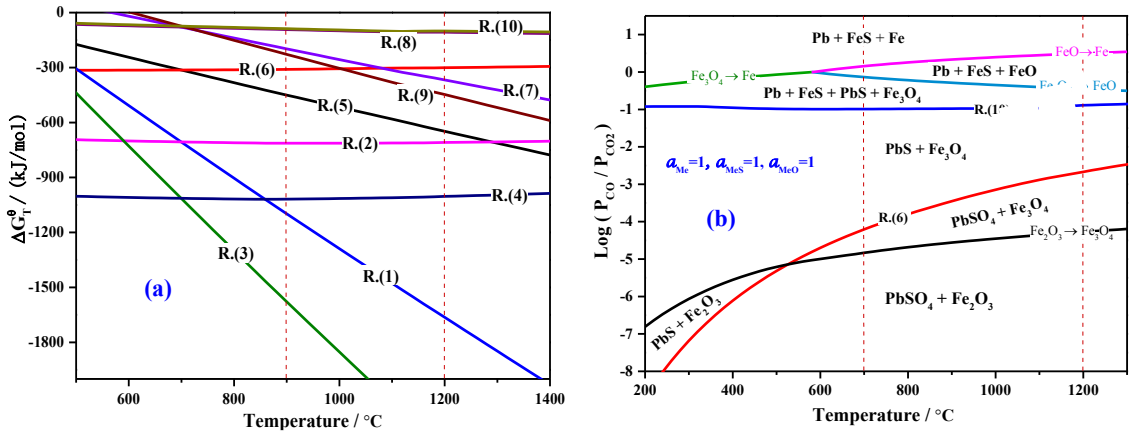

Fig. 4. The ΔG_T^θ and T diagram of reactions (1)-(10) and a reductive sulfur-fixing equilibrium diagram of $PbSO_4$ and Fe_2O_3.

HSC version 9.2.6 (Roine, 2002) was employed for the thermodynamic calculation of the above reactions. Figure 4(a) shows a ΔG_T^θ vs. T diagram of reactions (1)-(10). It indicates that extraction of metallic lead is thermodynamically favorable in a temperature range of 900-1200°C, in the presence of Fe_2O_3 and a reductant. Increasing the temperature will promote reactions (1), (3), (5), (7), and (9).

The reductive equilibrium diagram of $PbSO_4$ and Fe_2O_3 presented in Figure 4(b) further illustrates that seven stability regions exist in reducing atmospheres. $PbSO_4$ is easily reduced to PbS in weakly reducing conditions. In the same domain, Fe_2O_3 will also be reduced to Fe_3O_4. Therefore, reactions (1)-(4) and (7)-(8) do not advance during smelting. As P_{CO}/P_{CO_2} and temperatures are increased, Pb extraction reactions take place between PbS and Fe_3O_4. Within that domain, metallic Pb, FeS, PbS, and Fe_3O_4 will coexist. Sulfur will transfer from PbS to FeS and finally become fixed as sulfide matte.

4. Results and discussion

4.1 $PbSO_4$ reaction behavior

The XRD patterns of $PbSO_4$ at different reaction temperatures and times are shown in Figure 5. It is apparent from Figure 5(a) that $PbSO_4$ was stable and did not decompose below 879°C (1152 K), nor even at 900°C (1173 K) in an inert atmosphere. Combined with the TG-DTA analysis, the X-ray patterns indicated that volatilization of $PbSO_4$ was the main reaction. However, at 971°C (1243 K), the decomposition of $PbSO_4$ was identified, producing $PbO{\cdot}PbSO_4$. As the temperature rose to 1000°C (1273 K), the decomposition product PbO from $PbO{\cdot}PbSO_4$ was increasingly converted to metallic Pb.

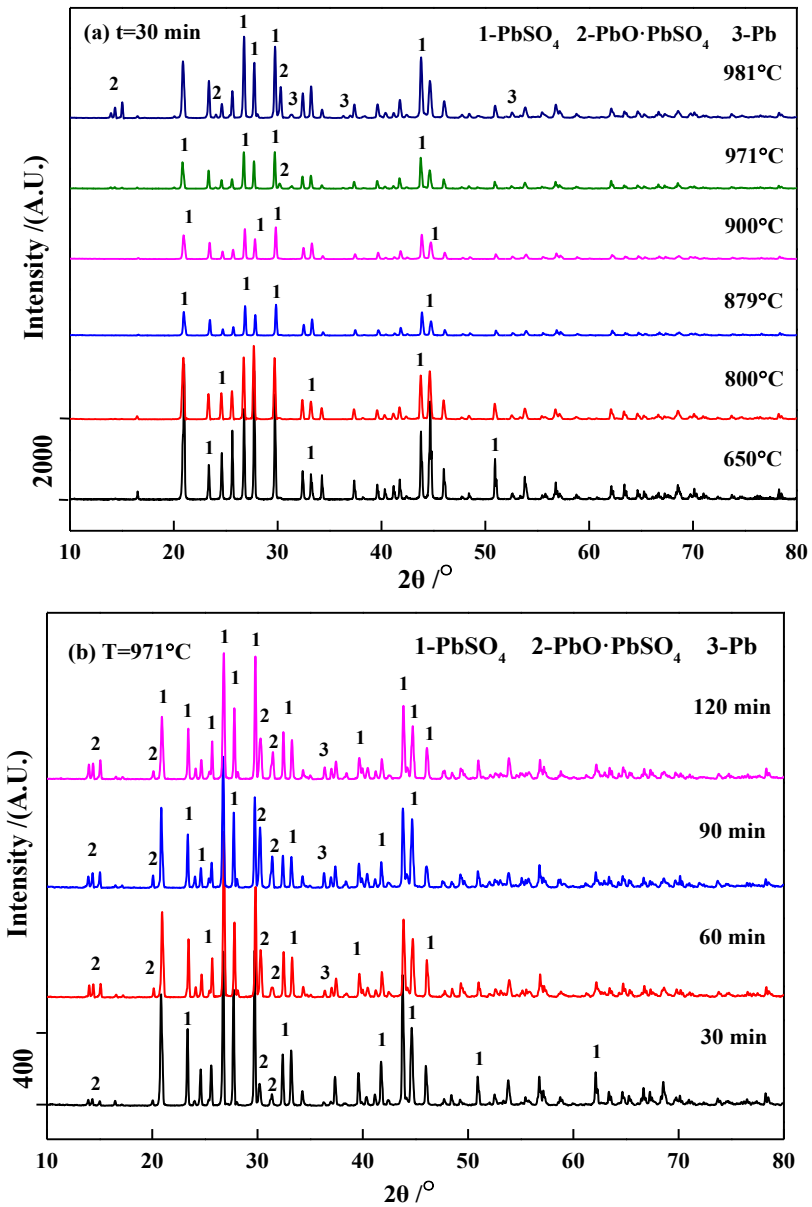

Fig. 5. XRD patterns of $PbSO_4$ (a) at different temperatures and (b) after different reaction times.

Figure 5(b) illustrates the phase evolution of $PbSO_4$ at 971°C (1243K) as a function of reaction time. It indicates that the decomposition $PbSO_4 \rightarrow PbO{\cdot}PbSO_4$ advanced with increasing reaction time. Metallic Pb was detected after 1 h and its diffraction peak intensity rose gradually as the process time was extended.

4.2 $PbSO_4$-C mixture reaction behavior

Figure 6 shows the XRD patterns of the $PbSO_4$-C mixture at different temperatures and times. Figure 6(a) proves that $PbSO_4$ did not decompose in the reducing atmosphere at 500°C (773 K) and remained stable after 30 min reaction time. $PbO{\cdot}PbSO_4$ was detected at approximately 650°C (923 K). It appears that the

presence of carbon promotes the decomposition and reduction of $PbSO_4$. When the temperature was increased to 760°C (1033 K), the diffraction peak intensity of $PbO{\cdot}PbSO_4$ increased. At 800°C (1073 K), $PbSO_4$ and $PbO{\cdot}PbSO_4$ disappeared completely, and new products, $2PbO{\cdot}PbSO_4$, Pb, and PbS, emerged. This indicates that a part of the $PbSO_4$ was reduced to PbS. With the increase in temperature, the decomposition reaction intensified until $2PbO{\cdot}PbSO_4$ disappeared at 850°C (1123 K), and $4PbO{\cdot}PbSO_4$, Pb, and PbS appeared. Above 850°C (1123 K), the diffraction peak intensity of PbS decreased and that of Pb increased with increasing temperature. This indicates that the fraction of metallic Pb in the product increased and PbS reduced gradually.

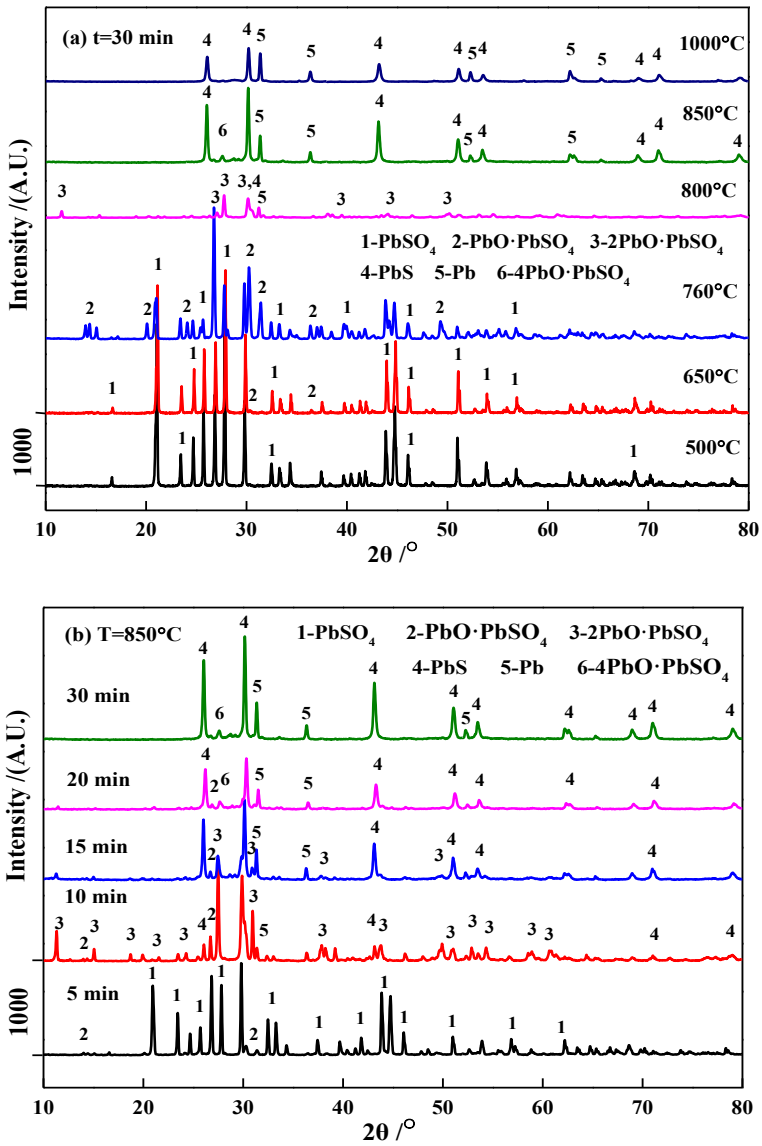

Fig. 6. XRD patterns of the $PbSO_4$-C mixture (molar ratio 1:6) (a) at different temperatures and (b) after different reaction times.

Figure 6(b) illustrates the XRD patterns of the $PbSO_4$-C mixture at 850 °C (1123 K) for different reaction times. It shows that, at 850°C (1123 K), $PbSO_4$ quickly decomposed to $PbO{\cdot}PbSO_4$, within 5 min, in the presence of carbon. After 10 min, $PbSO_4$ was replaced by $PbO{\cdot}PbSO_4$ and $2PbO{\cdot}PbSO_4$. Some lead sulfate was also reduced to PbS, and the generated lead oxide was reduced further to metallic Pb. When smelting time was extended to 15 min, the diffraction peak intensities of $PbO{\cdot}PbSO_4$ and $2PbO{\cdot}PbSO_4$ decreased gradually, but the intensities of PbS and Pb increased. After 20 min smelting, the generation of lead oxide in the product continued and $4PbO{\cdot}PbSO_4$ appeared. After 30 min, the product mainly comprised PbS, Pb, and a small fraction of $4PbO{\cdot}PbSO_4$.

When comparing the results in the $PbSO_4$-C and $PbSO_4$ systems, it is apparent that, at low temperatures and weakly reducing atmospheres, $PbSO_4$ decomposed to $PbO{\cdot}PbSO_4$, and $2PbO{\cdot}PbSO_4$. At the same time, a small fraction of $PbSO_4$ was reduced to PbS. Later, intermediate products $xPbO{\cdot}PbSO_4$ (x=1 or 2) continued to produce $4PbO{\cdot}PbSO_4$. At high temperatures, $PbSO_4$ was directly reduced to PbS. In such conditions, the intermediate products $xPbO{\cdot}PbSO_4$ (x=1, 2 or 4) would also decompose into PbO and reduce to metallic Pb. The final products were PbS and Pb. Therefore, a reductive atmosphere and the smelting temperature are the key factors affecting the efficiency of lead recovery and sulfur fixation. A sufficiently reductive atmosphere can selectively reduce $PbSO_4$ to PbS, as shown above. These reactions guarantee sulfur fixation in the smelting system without formation of $SO_{2(g)}$ or $SO_{3(g)}$, and the subsequent discharge of sulfur into the atmosphere in the process off-gas.

4.3 $PbSO_4$-Fe_2O_3-C mixture reaction behavior

Figure 7 presents the XRD patterns of the $PbSO_4$-Fe_2O_3-C mixture at different temperatures and times. Figure 7(a) shows that the exchange reactions between $PbSO_4$ and Fe_2O_3 did not occur at low temperatures, typically below 650°C (923 K), within 30 min, even if a reductant was present. $PbSO_4$ was reduced to PbS in reducing atmospheres, as at 750°C (1023 K) PbS was detected in the reaction products. When the temperature was increased to 850°C (1123 K), $PbSO_4$ also decomposed to $PbO{\cdot}PbSO_4$, while iron oxides remained in the system as Fe_2O_3. However, at 950°C (1223 K), Fe_2O_3 was reduced to Fe_3O_4. In addition, the decomposition product PbO reacted with Fe_2O_3, forming $PbFe_{12}O_{19}$. As the temperature was increased, $PbSO_4$ disappeared and metallic Pb appeared at

1000°C (1273 K). The products were PbS, Pb, Fe_3O_4, and $PbFe_{12}O_{19}$. Above 1100°C (1373 K), secondary products, such as $PbFe_8O_{13}$, $Pb_2Fe_2O_5$, Pb_2O_3, and FeS, were detected. At the same time, metallic Pb beads were generated and separated from the reaction mixture. Therefore, the diffraction peaks of Pb were not found in the XRD patterns. The final products of the conversion reactions were Pb, Fe_2O_3, $PbFe_8O_{13}$, $Pb_2Fe_2O_5$, Pb_2O_3, and FeS.

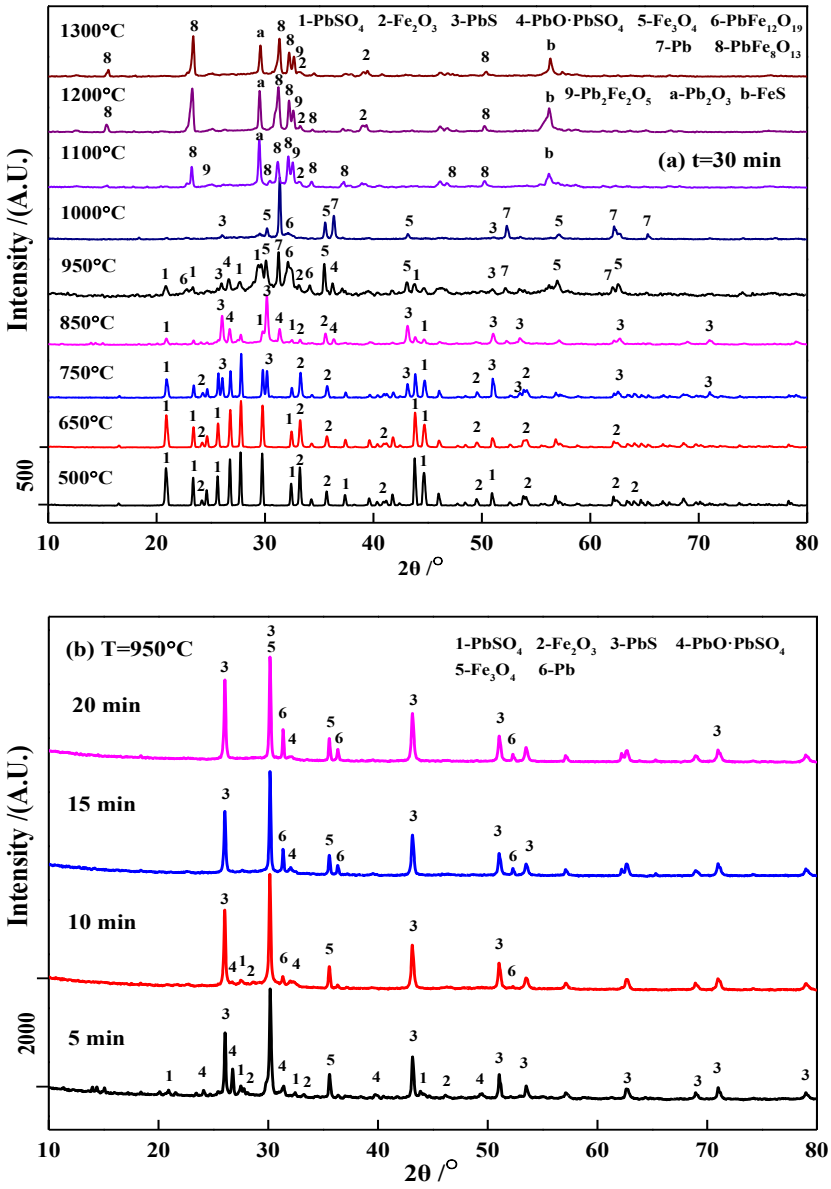

Fig. 7. XRD patterns of the $PbSO_4$-Fe_2O_3-C (molar ratio 2:1:12) mixture (a) at different temperatures and (b) after different reaction times.

Combined with the XRD results of $PbSO_4$ shown in Figure 7(b) and the results of $PbSO_4$-C mixture shown in Figure 6(b), Figure 7(b) further proved that at 950°C (1223 K) $PbSO_4$ was reduced to PbS within 5 min. Fe_2O_3 was also reduced to Fe_3O_4.

Metallic Pb was detected after 10 min reaction. However, before this time, neither Fe_2O_3 nor Fe_3O_4 was involved in Pb generation, as no FeS was detected. This suggests that some metallic Pb was generated through the sequence $PbSO_4 \rightarrow PbO{\cdot}PbSO_4 \rightarrow 2PbO{\cdot}PbSO_4 \rightarrow 4PbO{\cdot}PbSO_4 \rightarrow PbO \rightarrow Pb$ by gas-solid processes.

The appearance of FeS in Figure 7(a) implies that, below approximately 1100°C (1373 K), an exchange reaction occurred between PbS and iron oxide, evidently Fe_3O_4, producing FeS and PbO. The possible reactions (Roine, 2002) are:

$$2PbS_{(l)}+Fe_2O_3+C=2PbO_{(l)}+2FeS_{(l)}+CO_{(g)} \qquad \Delta G_T^{\theta} = -0.064\ T + 69.604 \qquad (11)$$

$$2PbS_{(l)}+Fe_2O_3+CO_{(g)}=2PbO_{(l)}+2FeS_{(l)}+CO_{2(g)} \qquad \Delta G_T^{\theta} = -0.022\ T+40.263 \qquad (12)$$

$$3PbS_{(l)}+Fe_3O_4+C=3PbO_{(l)}+3FeS_{(l)}+CO_{(g)} \qquad \Delta G_T^{\theta} = -0.068\ T + 95.72 \qquad (13)$$

$$3PbS_{(l)}+Fe_3O_4+CO_{(g)}=3PbO_{(l)}+3FeS_{(l)}+CO_{2(g)} \qquad \Delta G_T^{\theta} = -0.026\ T+66.38 \qquad (14)$$

The Gibbs energies of reactions (11)-(14) are expressed in kJ/mol, and temperatures are in °C.

It is evident from the XRD patterns of the $PbSO_4$-Fe_2O_3-C mixture that the presence of carbon facilitated the exchange reactions between $PbSO_4$ and Fe_2O_3 and ultimately generated metallic Pb and ferrous sulfide.

SEM-EDS analyses were employed to detect the microstructures, element distributions, and transformation mechanism of the $PbSO_4$-Fe_2O_3-C reaction system at 950°C (1223 K) and 1000°C (1273 K) after 30 min reaction. The results are presented in Figures 8(a)-(d).

As shown in Figure 8, ferric oxide Fe_2O_3 (area D) was surrounded by magnetite Fe_3O_4 (area E), which indicates that the reduction of Fe_2O_3 advanced at 950°C (1223 K) within 30 min. At the same time, the intermediate product PbS (B areas) was detected, but it gradually declined with increasing temperature due to the exchange reactions between PbS and Fe_3O_4. Furthermore, it was observed (see Figure 8) that metallic Pb droplets (A areas) were often close to PbO minerals (F areas) and PbS particles. Pb, PbO, and PbS grains were generally surrounded by lead iron oxides ($Pb_2Fe_2O_5$, $PbFe_8O_{13}$, or $PbFe_{12}O_{19}$, areas C). FeS domains (G areas) were detected around PbS and lead iron oxides. This proves that metallic Pb was generated through reduction of PbO. Moreover, the generation of PbO depended on the exchange reactions between PbS and Fe_3O_4. In addition, unreacted PbO had infiltrated the pores of Fe_3O_4 and Fe_2O_3 because of its low melting point (886°C (1159 K)). As a result, some PbO had combined with Fe_2O_3 to form $PbFe_xO_y$ (x=2, 8

or 12 etc.), as shown in the C areas in Figure 8. A brighter color in the C areas means a higher PbO concentration.

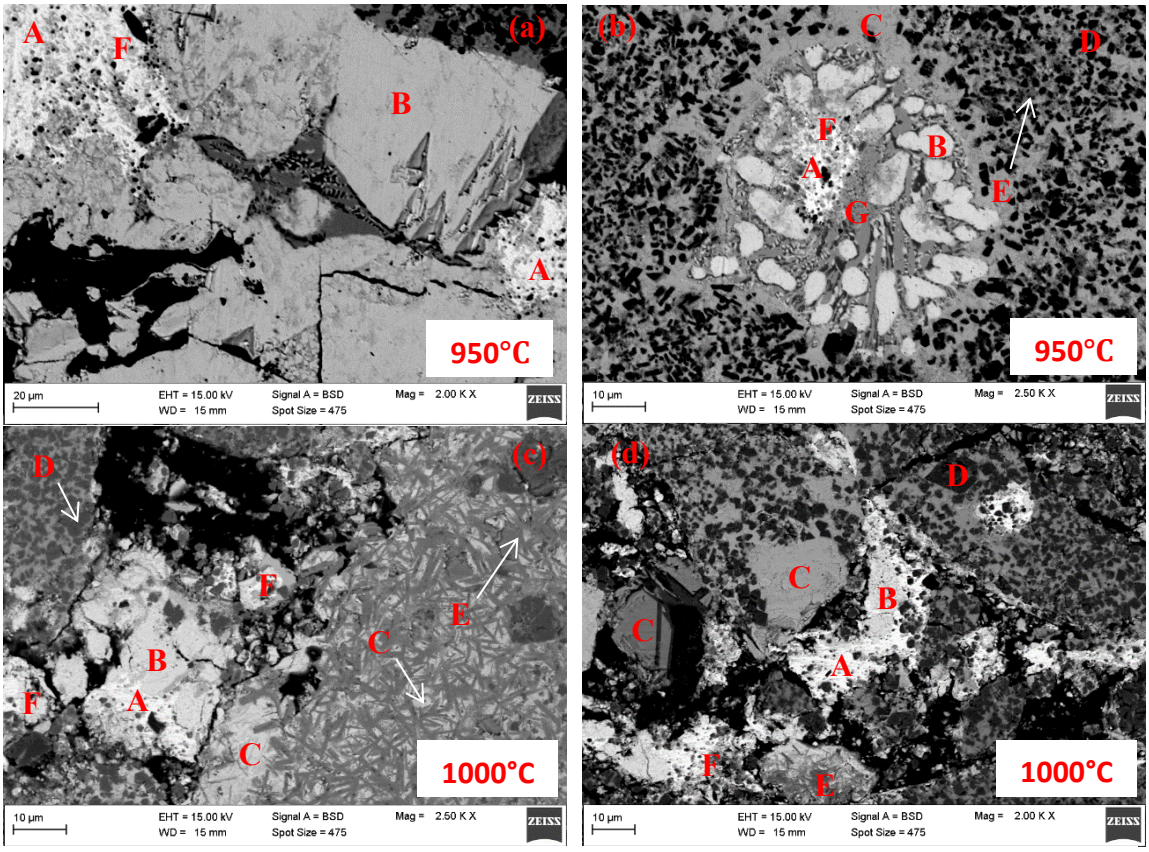

A: Metallic lead (Pb); **B**: Lead sulfide (PbS); **C**: Lead iron oxide ($PbFe_xO_y$); **D**: Ferric oxide (Fe_2O_3); **E**: Magnetite (Fe_3O_4); **F**: Lead monoxide (PbO); **G**: Ferrous sulfide (FeS)

Fig. 8. SEM micrographs of products in the $PbSO_4$-Fe_2O_3-C (molar ratio 2:1:12) mixture at 950°C and 1000°C after 30 min reaction time

The above TG-DTA, XRD, and SEM-EDS results suggest that recycling lead from lead paste using iron oxide as the sulfur-fixing agent is fundamentally and technically possible. The presence of a reductant was essential and promoted the reduction-decomposition of $PbSO_4$ to PbS. It also facilitated the exchange reactions between PbS and iron oxide to produce PbO and FeS. As a result, PbO was reduced to metallic Pb. These results agree well with the thermodynamic calculations presented in Figure 3(b). The detailed reactions and conversion mechanisms of $PbSO_4$-Fe_2O_3-C smelting are illustrated in Figure 9.

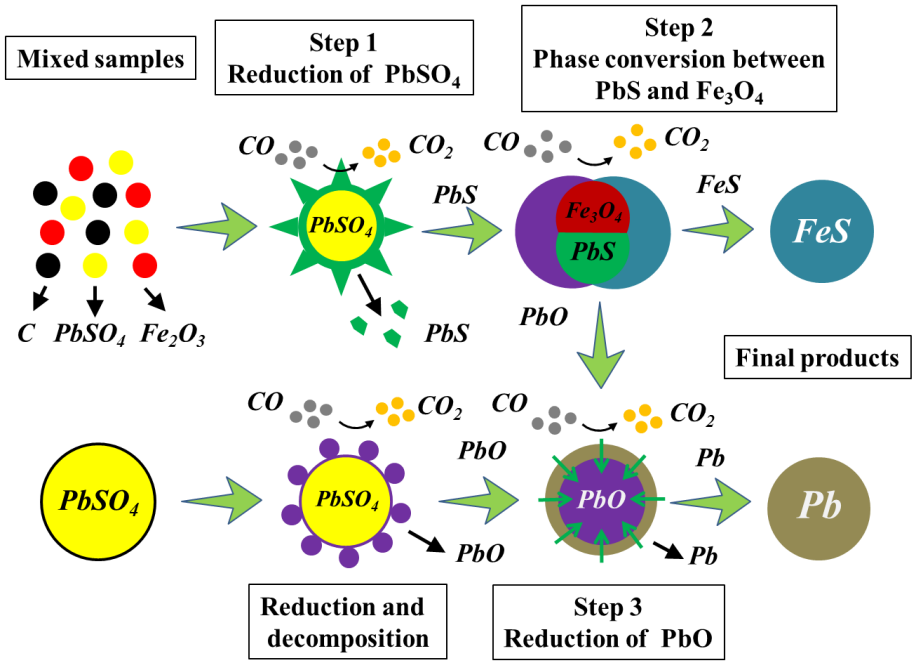

Fig. 9. Phase transformation mechanism in the reductive sulfur-fixing process of lead acid battery paste recycling.

As the conversion mechanism of reducing LAB paste smelting, $PbSO_4$ is first reduced to PbS, forming a small amount of lead oxide at a relatively low temperature. Next, the intermediate sulfide product, PbS, reacts with iron oxide to produce PbO and FeS. PbO is also constantly reduced to metallic Pb. With the help of the exchange reactions, the sulfur in $PbSO_4$ is transferred to PbS, and is finally fixed and stabilized as FeS, which prevents the generation and emissions of SO_2 gas.

4.4 Process optimization investigation and industrial pilot campaign

Figure 10 illustrates the effects of coke addition in the lab-scale batch experiments on lead recovery and sulfur-fixing rate in reductive sulfur-fixing smelting. The lead recovery and sulfur-fixing rate increased gradually along with the coke dosage and peaked at addition of 14% coke. In these conditions, 92.7% of the lead was recovered to crude lead and 96.9% of the sulfur was fixed in a ferrous matte and slag. When coke dosage was further increased, lead recovery and sulfur-fixing rate remained constant at around 93% and 97%, respectively. This indicates that a reducing atmosphere is essential for lead recovery and sulfur fixation. Optimized additions of coke thus improve lead extraction and sulfur fixation.

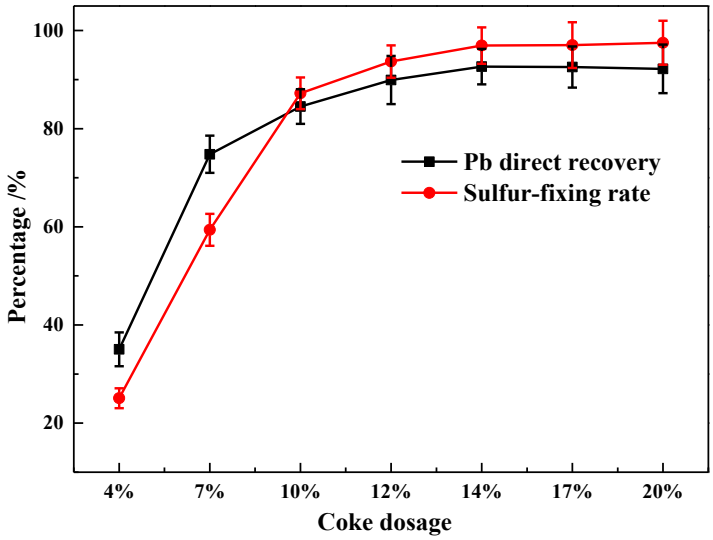

Fig. 10. The effects of coke dosage on lead recovery and sulfur-fixing rates ($W_{lead\ paste}$: $W_{hematite}$=300:60 g. FeO/SiO_2=1.3, CaO/SiO_2=0.4, 1200°C, 2 h).

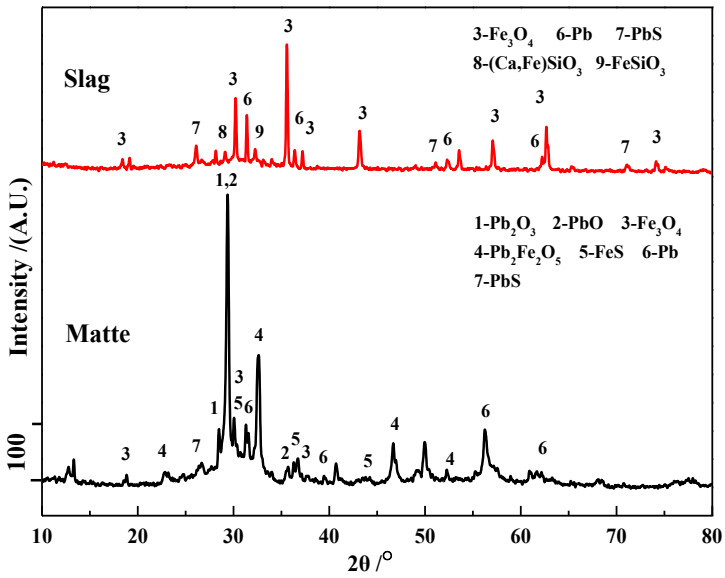

Fig. 11. XRD patterns of matte and slag products at 1200 °C ($W_{lead\ paste}$: $W_{hematite}$: W_{coke}=300:60:12 g. FeO/SiO_2=1.3, CaO/SiO_2=0.4, 2 h).

Figure 11 shows the XRD patterns of the products with additions of 4% coke and 20% hematite. Lead sulfide (PbS) and lead oxides (Pb_2O_3, PbO, and $Pb_2Fe_2O_5$) were detected in the matte, which indicates that insufficient coke additions cannot provide acceptable lead recovery. Metallic lead was also detected, entrained in the matte and slag. This implies that settling of metallic lead was poor in a weakly reductive atmosphere and some lead was lost in matte and slag. Fe_3O_4 and PbS were detected at the same time in the matte, indicating that the reductive sulfur-fixing reactions between Fe_3O_4 and PbS were unsatisfactory. An optimized addition of reductant is required to facilitate the reactions, improve the settling,

and increase the recovery of metallic lead. These results agree well with the thermodynamic constraints mentioned above.

The influence of hematite addition on the lead recovery and sulfur-fixing rates is presented in Figure 12, which illustrates that lead recovery rose from 58% to 93%, and sulfur fixation from 60% to 97% with increasing addition of sulfur-fixing agent. An appropriate hematite feed thus promoted lead recovery and sulfur fixation. A further increase in hematite feed showed no increase in lead recovery or sulfur-fixing rate.

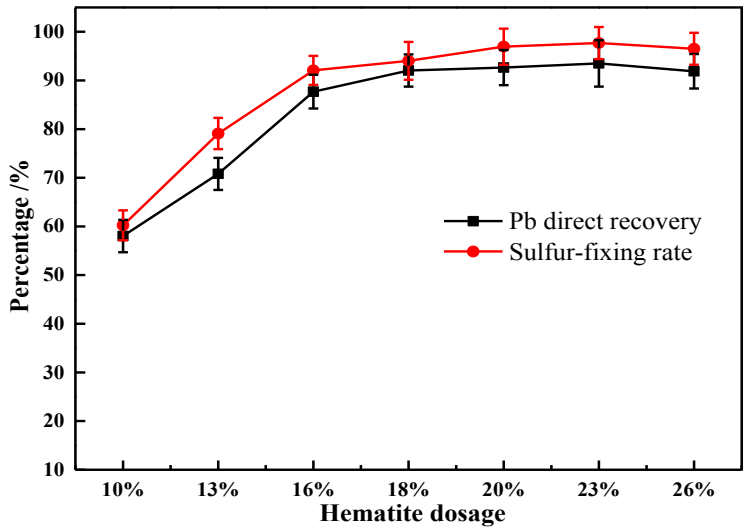

Fig. 12. The effects of hematite dosage on lead recovery and sulfur fixation ($W_{lead\ paste}$: W_{coke} =300:42 g. FeO/SiO_2=1.3, CaO/SiO_2=0.4, 1200°C, 2 h).

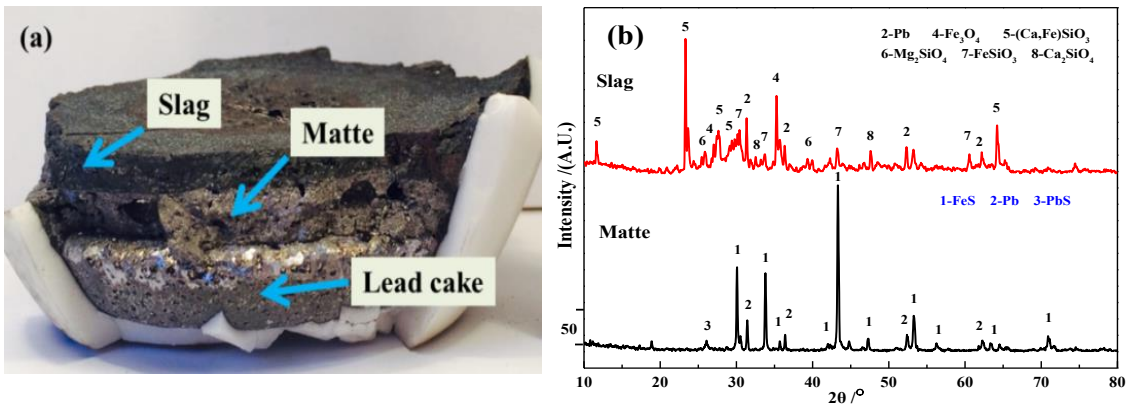

Fig. 13. (a) Physical macrograph and (b) XRD patterns of the matte and slag ($W_{lead\ paste}$: $W_{hematite}$: W_{coke}=300:60:42 g. FeO/SiO_2=1.3, CaO/SiO_2=0.4, 1200°C, 2 h).

Figure 13(a) presents a macrograph of the smelting products at 1200°C, with 14% addition of coke, 20% hematite addition, and 2 h reaction time. It shows that the products were separated into three distinct layers: slag, ferrous matte, and crude lead. Slag floats on the surface of the ferrous matte, and metallic Pb settles at

the bottom of the crucible due to density differences. Figure 13(b) shows the XRD patterns of the matte and slag. It shows that FeS was the major constituent of the matte, and only small diffraction peaks of Pb and PbS were detected. The lead oxides detected earlier, see Figure 11, had disappeared. This implies that most PbS had reacted with Fe_xO_y to generate metallic Pb, and the settling of lead had also improved. The 14% coke and 20% hematite additions provided a sufficient sulfur-fixing atmosphere to recover metallic lead. The slag comprised Fe_3O_4, $(Ca,Fe)SiO_3$, Mg_2SiO_4, $FeSiO_3$, and Ca_2SiO_4. However, there was still some metallic lead entrained and lost in the slag. A longer settling time would be needed to decrease mechanical lead losses in the matte and slag.

The industrial-scale experiments were conducted in a 4 m^3 blast furnace. The flowsheet used is presented in Figure 14. Various lead-bearing secondary materials, including LAB paste, lead dust, lead sludge, and lead slag, were mixed carefully and briquetted with iron-bearing wastes, including pyrite cinder and jarosite residue, to obtain a mixture containing 30% Pb, 8% S, and 25% Fe. 1200 kg of dry briquettes were fed into the blast furnace with an appropriate amount of coke and fluxes (silica sand and limestone). The smelting products, i.e., crude lead, matte, and slag, were discharged through their corresponding tap holes. Matte was laundered together with slag and settled in cast iron molds. The slag floated on the surface of the matte, preventing oxidation. After tapping, the slag was quenched in a water pool.

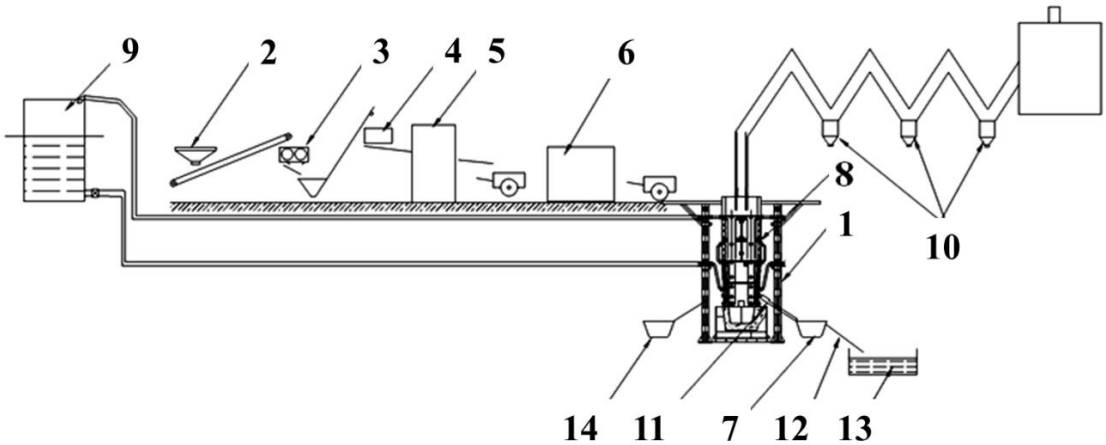

1. blast furnace, 2. feed hopper, 3. roller machine, 4. blender, 5. briquetting machine, 6. dry storage yard, 7. cast matte and slag molds, 8. water jacket, 9. power-loss circulating water cooling, 10. cyclone dust collector, 11. water-cooled launder, 12. slag launder, 13. quenching water pool, 14. cast lead molds.

Figure 14. Flowsheet of the industrial pilot trial campaign.

The results of the industrial pilot campaign are collected in Figures 15 and 16 and Tables 3 and 4. Figure 15 shows that the lead content of the sulfide matte was approximately 4%-5%, and that the lead content of the slag decreased to 1-2% within one hour. The grade of crude lead produced was 96%-98% Pb. Table 3 and Figure 16 indicate that 90-96% of the lead can be recovered in one step into crude lead. 97-99% of the sulfur in the feed was fixed in the condensed state, instead of generating and emitting SO_2 gas. The Pb recovery rate in Table 3 is the sum of lead in the crude lead and matte; the dust rate was calculated according to the mass of dry briquettes and the sulfur-fixation rate was measured from the sulfur content of the off-gas.

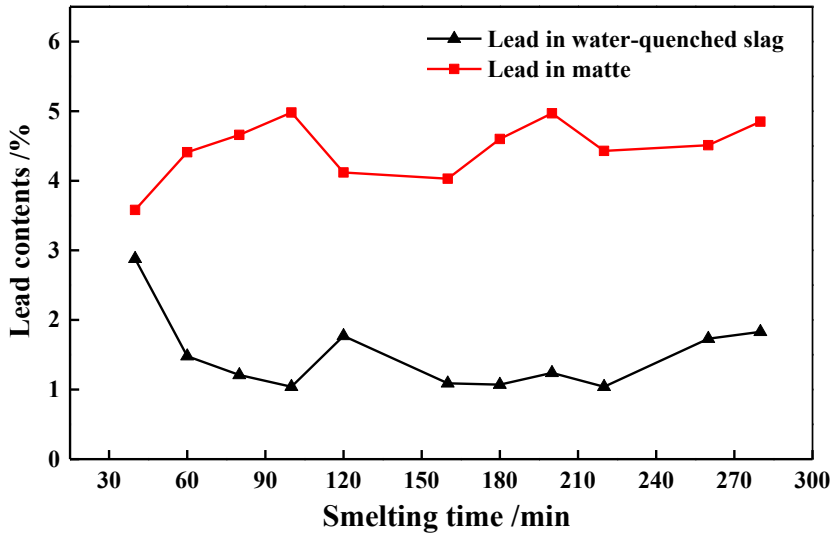

Figure 15. Pb content in the matte and slag during industrial production trial (1150-1200°C).

Table 3. The key technical parameters of the industrial pilot campaign.

Production intensity /(kg/ (m²·d))	Direct Pb recovery /%	Total Pb recovery /%	Coke addition /%	Dust rate /%	Sulfur-fixation rate /%	Coke consumption /(kg/t Pb)	Limestone consumption /(kg/t Pb)
21000-33000	87-92	90-96	12-16	3-6	97-99	420-600	200-500

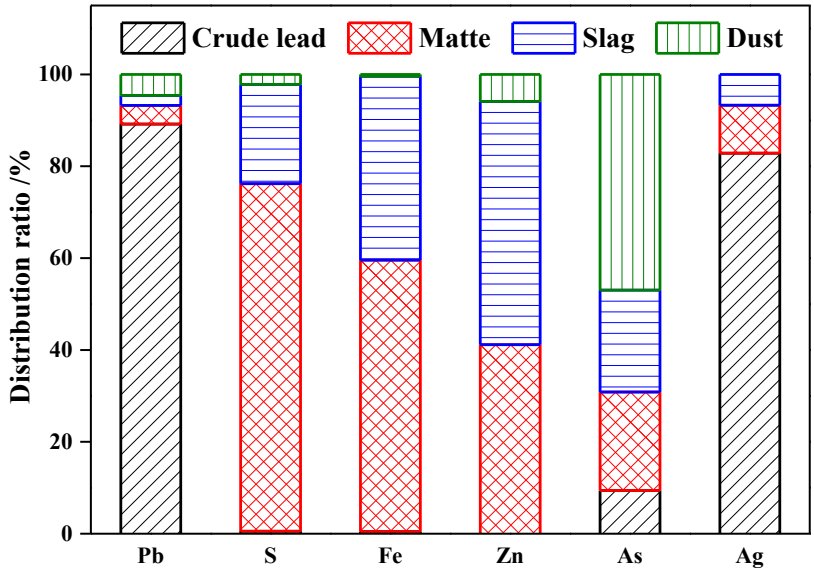

Figure 16. Distribution behavior of the main components during the industrial pilot campaign /%.

Compared with the lab-scale results under "ideal" conditions, it is evident that more sulfur was fixed in the industrial-scale pilot experiment. The industrial pilot campaign also revealed that this novel process can be executed on a continuous basis and offers advantages, e.g., in terms of low dust generation and high production capacity.

Table 4 shows the monitoring results of the blast furnace off-gas. It clearly reveals that all the emission targets meet the standard GB 25466-2010 (National standard of P.R. China --- Emission Standard of Pollutants for Lead and Zinc Industry).

Table 4. The blast furnace off-gas monitoring results during the pilot trial.

Location of monitoring point	Monitored parameters	Monitoring results				Executive standard
Blast furnace smoke window	Pb / (mg/m^3)	0.046	0.041	0.034	0.037	0.5
	SO_2 / (mg/m^3)	380	363	354	372	400
	Cd / (mg/m^3)	0.00019	0.00017	0.00021	0.00016	0.05
	Blackness	<1	<1	<1	<1	<1
	Air volume flow/(m^3/h)	18040	20240	21860	19872	--

5. Conclusions

The recycling and extraction of lead from lead acid battery paste using iron-bearing waste as sulfur-fixing agent was found to be fundamentally and technically

feasible. The phase conversion mechanisms of the smelting process were clarified. Metallic Pb was extracted from the $PbSO_4$ in lead paste mainly through the sequence of $PbSO_4 \xrightarrow{C/CO} PbS \xrightarrow{Fe_3O_4} PbO \xrightarrow{C/CO} Pb$. Sulfur transferred from $PbSO_4$ to FeS and was fixed in the smelting system as sulfide matte, which eliminated emissions of gaseous SO_2.

The lab-scale experiments illustrated that 93% of lead in the raw material could be recovered in crude lead and that 97% sulfur was fixed in ferrous matte. The industrial pilot campaign revealed that the new process could be operated continuously. It was possible to recover 90-96% of lead in one step into crude lead. The lead content of matte and slag was around 4-5 % and 1-2 %, respectively. The sulfur-fixation rate reached 97-99 %. In addition to LAB scrap, the process can treat various metallurgical and hazardous wastes and recycle a variety of valuable metals included in them. The off-gas emissions met the relevant Chinese standards. This process offers multiple application prospects in the field of secondary lead recycling.

Acknowledgements

This work was supported by the Guangdong Provincial Applied Science and Technology Specialized Research Project [Grant No. 2016B020242001], the Hunan Provincial Science Fund for Distinguished Young Scholars [Grant No. 2018JJ1044], the National Natural Science Foundation of China [Grant No. 51234009 and 51604105], CMEco [Grant No. 2116781] by Business Finland, the Fund for Less Developed Regions of the National Natural Science Foundation of China (Grant No. 51664013), the Program for Young Talents of Science and Technology in Universities of the Inner Mongolia Autonomous Region (Grant No. NJYT-17-B35), and the Bayannur Science and Technology Project from the Bayannur Bureau for Science and Technology (Grant No. K201509).

References

Andrews, D., Raychaudhuri, A. and Frias, C., 2000. Environmentally sound technologies for recycling secondary lead. J. Power Sources, 88(1): 124-129.

Dahodwalla, H. and Herat, S., 2000. Cleaner production options for lead-acid battery manufacturing industry. J. Clean. Prod., 8(2): 133-142.

Ellis, T.W. and Mirza, A.H., 2010. The refining of secondary lead for use in advanced lead-acid batteries. J. Power Sources, 195(14): 4525-4529.

Gong, C., Zhang, X., Hu,Q., Chen, Y., Fang, M., Zhang, H., Chen, Q., and Lei, L., 2015. Research Progress of Desulphurization Methods for Scrap Lead Paste. Int. J. Chem. and Mater. Res., 3(3): 58-64.

Guangdong Xinsheng Environmental Science & Technology Co., L., Chaozhou, China, 2014. Company profile and technical process. http://www.xsept.cn/.

Guoda Nonferrous Metals Smelting Co., L., Chenzhou, China, 2009. Company profile. http://www.czgdys.com.cn.

Higgins, C.J., 2007. Quantifying and Assessing the Impacts of Heavy Metal Flows: Fate, Transport, and Impacts of Lead Use in US Product Manufacturing, Carnegie Mellon University, Pittsburgh, PA.

Hotea, V., 2013. Clean Technology of Lead Recovery from Spent Lead Paste. Recent Researches in Applied Economics and Management, Econ. Asp. of Environ., 2: 263-270.

Huang, C,. Tang, C., Tang, M., Yang, J., Chen, Y., Yang S., and He, J., 2012. Sulfur-fixing Reduction Smelting of Spent Lead-acid Battery Colloid Sludge in Fused Salt at Low Temperature. Min.and Metall. Eng., 32(2): 84-87.

Jaeck, M.L., 2013. Primary and Secondary Lead Processing: Proceedings of the International Symposium on Primary and Secondary Lead Processing, Halifax, Nova Scotia, August 20-24. Elsevier.

Jeong, K.-P. and Kim, J.G., 2017. Lead acid battery recycling and material flow analysis of lead in Korea. J. Mater. Cy. and Waste Manag. 20: 1348-1354.

Karandikar, A.S.P.B., 2015. Review on Desulfation of Lead-acid Battery for HEV. International Journal of Current Engineering and Scientific Reasearch (IJCESR), 2(9): 2393-8374.

Kreusch, M.A., Ponte, M. J. J. S., Ponte, H. A., Kaminari, N. M. S., Marino, C. E. B., and Mymrin, V., 2007. Technological improvements in automotive battery recycling. Resour. Conserv. & Recy., 52(2): 368-380.

Li, Y., Tang, C., Chen, Y., Yang, S., Guo, L., He, J. and Tang, M., 2017. One-Step Extraction of Lead from Spent Lead-Acid Battery Paste via Reductive Sulfur-Fixing Smelting: Thermodynamic Analysis, 8th International Symposium on High-Temperature Metallurgical Processing. Springer, in: Hwang JY. et al. (eds). TMS. Springer, Cham, pp. 767-777.

Lin, D. and Qiu, K., 2011. Recycling of waste lead storage battery by vacuum methods. Waste Manag., 31(7): 1547-1552.

Ma, C., Shu, Y. and Chen, H., 2016. Preparation of high-purity lead oxide from spent lead paste by low temperature burning and hydrometallurgical processing with ammonium acetate solution. RSC Adv., 6(25): 21148-21155.

Pan, J., Zhang, X., Sun, Y., Song, S., Li, W., Wan, P., 2016. Preparation of high purity lead oxide from spent lead acid batteries via desulfurization and recrystallization in sodium hydroxide. Ind. & Eng. Chem. Res., 55(7): 2059-2068.

Queneau, P.B., Leiby, R. and Robinson, R., 2015. Recycling lead and zinc in the United States. Zinc and lead processing. Montreal: The Metallurgical Society of CIM, 68 (3): 149-161.

Roine, A., 2002. HSC Chemistry 9.0. Outokumpu Research Oy, Pori, Finland.

Schröder-Wolthoorn, A., Kuitert, S., Dijkman, H. and Huisman, J.L., 2008. Application of sulfate reduction for the biological conversion of anglesite ($PbSO_4$) to galena (PbS). Hydrometallurgy, 94(1): 105-109.

Singh, A., 2015. Review on Desulfation of Lead-acid Battery for HEV. Int. J. Curr. Eng. and Sci. Res., 2(9): 85-96.

Sonmez, M. and Kumar, R., 2009. Leaching of waste battery paste components. Part 1: Lead citrate synthesis from PbO and PbO_2. Hydrometallurgy, 95(1): 53-60.

Tang, C., Tang, M., Yao, W., Ruan, Y. and Peng, J., 2004. Pilot test of reduction-matting smelting of jamesonite concentrate with short rotary furnace. Min. and Metall. Eng., 24(1): 51-53.

Tian, X., Gong, Y., Wu, Y., Agyeiwaa, A. and Zuo, T., 2014. Management of used lead acid battery in China: Secondary lead industry progress, policies and problems. Res. Conserv. & Recy., 93(93): 75-84.

Tian, X., Wu, Y., Gong, Y. and Zuo, T., 2015. The lead-acid battery industry in China: outlook for production and recycling. Waste Manag. & Res., 33(11): 986-994.

Tian, X., Wu, Y., Hou, P., Liang, S., Qu, S., Xu, M., & Zuo, T., 2017. Environmental impact and economic assessment of secondary lead production: Comparison of main spent lead-acid battery recycling processes in China. J. Clean. Prod., 144: 142-148.

Toby, B., 2005. CMPR - a powder diffraction toolkit. J. Appl. Crystallogr., 38(6): 1040-1041.

Van der Kuijp, T.J., H., L. and Cherry, C.R., 2013. Health hazards of China's lead-acid battery industry: a review of its market drivers, production processes, and health impacts. Environ. Health, 12(1): 61.

Wei, J., Guo, X., Marinova, D. and Fan, J., 2014. Industrial SO_2 pollution and agricultural losses in China: evidence from heavy air polluters. J. Clean. Prod.,, 64: 404-413.

Ye, L.G., Tang, C.B., Chen, Y.M., Yang, S.H., Yang, J.G., Zhang, W.H., 2015. One-step extraction of antimony from low-grade stibnite in Sodium Carbonate–Sodium Chloride binary molten salt. J. Clean. Prod., 93: 134-139.

Zhang, Q., 2013. The current status on the recycling of lead-acid batteries in China. Int. J. Electrochem Sci., 8: 6457-6466.